ACS OMEGA

http://pubs.acs.org/journal/acsodf

Article

Dopamine-Assisted Layer-by-Layer Deposition Providing Coatings with Controlled Thickness, Roughness, and Functional Properties

Runtian Qie, Saeed Zajforoushan Moghaddam, and Esben Thormann*

Cite This: *ACS Omega* 2023, 8, 2965−2972

Read Online

ACCESS | Metrics & More | Article Recommendations | Supporting Information

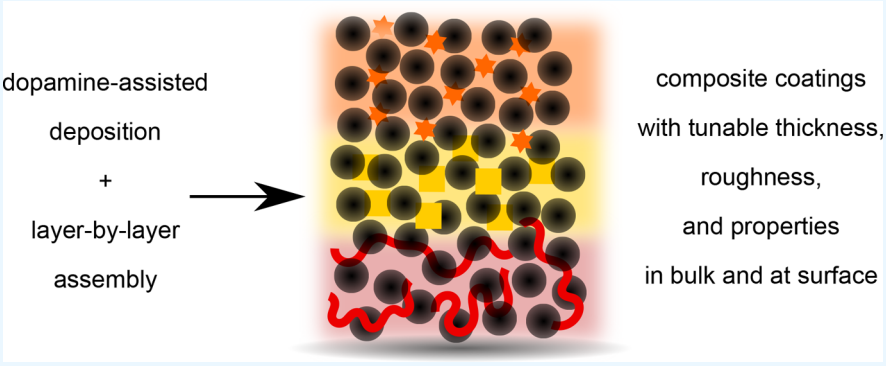

ABSTRACT: In this study, dopamine-assisted deposition combined with layer-by-layer assembly was investigated as an efficient method for preparing coatings with tunable thickness, roughness, and functional properties. By this method, one can first benefit from the versatile chemistry of dopamine allowing the co-deposition of various functional materials, for example, polymers, ions, and nanoparticles, within the coating. Moreover, the layer-by-layer approach allows tuning the coating thickness and surface roughness, as well as varying the chemical composition of the coating in the vertical direction. Herein, we demonstrated the benefits of using this method in fabricating both single- and multi-component coatings.

1. INTRODUCTION

Since the first report, in 2007, on the formation of polydopamine (PDA) coatings through self-polymerization in aqueous solutions, it has developed into a promising coating method owing to its simplicity and versatility.[1,2] Dopamine (DA) is a catecholamine that can be oxidized into DA-quinone, followed by intramolecular cyclization, oxidation to dopaminechrome, formation of 5,6-dihydroxyindole, and further oxidation to 5,6-indolequinone. These oligomers then undergo various covalent and non-covalent pathways self-assembling into supramolecular PDA structures in solution and at the surface.[3−5] Due to the highly reactive nature of these intermediate compounds, DA can also be co-deposited with various materials including polymers,[6−10] nanoparticles,[6,11] and metal ions,[12−14] whereby hybrid coatings with desired functionalities can be prepared. Despite the many benefits, preparing PDA-based coatings has challenges in controlling the coating growth and surface morphology. For example, the thickness of pure PDA coatings is usually limited to ∼50 to 100 nm due to the consumption of DA in the solution.[15−17] Moreover, the surface roughness of PDA coatings drastically increases with the deposition time due to aggregation, both in solution and at the surface.[18,19]

More than a decade before the rise of studies on PDA coatings, layer-by-layer (LbL) deposition was introduced as a versatile method of preparing polyelectrolyte multilayer coatings. Originally, multilayer coatings were formed by alternate deposition of oppositely charged polyelectrolytes (electrostatically assisted assembly) and tuning the coating properties by the polymers type, the number of depositions, and pH/ionic strength.[20,21] Later, the LbL deposition has been extended to include not only polyelectrolytes but also combinations of polyelectrolytes, nanoparticles, and lipids.[22−24] While other molecular interactions such as hydrogen bonding can also drive LbL assembly,[25,26] the electrostatically assisted assembly is still the most effective and used approach. Thus, despite the many advantages of the LbL method, the need for oppositely charged polymers is a limitation.

Considering the pros and cons of (i) DA-based deposition and (ii) LbL assembly of polyelectrolyte multilayers, the natural next step is to combine these methods to gain better control of the hierarchal structure of the coating as one has in the LbL process, while benefiting from the compositional tunability

Received: August 31, 2022
Accepted: December 29, 2022
Published: January 12, 2023

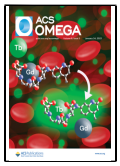

https://doi.org/10.1021/acsomega.2c05620
ACS Omega 2023, 8, 2965−2972

found in DA-based deposition. For pure PDA coatings, Ball and co-workers have reported an LbL approach, where a surface repeatedly was immersed in a fresh DA solution.[15,27] By doing so, they were able to extend the coating thickness beyond what is typically obtained, but a natural thought is that such an LbL approach should also affect the morphology of the PDA coatings. As the first part of our study, we thus extended this investigation into a study on both the growth rate and the surface morphology of PDA coatings fabricated with the LbL method. Few studies adopted an LbL approach to form multilayers of PDA and polymers/nanoparticles.[28−31] This method is generally executed by alternate adsorption of polymers/nanoparticles and PDA, whereby PDA layers practically work as a "glue" between the layers of polymers/nanoparticles. However, the LbL approach has been rarely combined with the elegant co-deposition approach for the formation of PDA-hybrid coatings. In the second part of our study, we thus investigated if co-deposition and LbL methods together can provide better control of the growth of PDA-polymer hybrid coatings. Specifically, we examined PDA-polyethyleneimine (PEI) hybrid films, where the assembly is driven by covalent PDA−polymer interactions, and PDA-dextran hybrid films, where the assembly is driven by noncovalent hydrogen bonding.

Besides a better control of the thickness and roughness, the most promising perspective of DA-assisted LbL deposition is the possibility of constructing hierarchically layered coatings by sequential deposition of layers with different compositions and functionalities, suitable for a wide range of surface modification applications.[32−34] For polyelectrolyte multilayer films, this has, for example, been done by adding a specific initial layer to promote adhesion of the coating to the substrate[35] or by adding a specific top layer to tune the surface properties.[36] As the third part of this study, we thus prepared a multilayer coating through DA-assisted deposition of polymers, nanoparticles, and ions using the LbL approach. It was demonstrated that DA-assisted LbL deposition allows preparing diverse hierarchal structures with tunable properties in bulk and at the surface of the coating.

2. MATERIALS AND METHODS

2.1. Materials. DA hydrochloride, tris(hydroxymethyl)-aminomethane (> 99.9%), PEI (branched, $M_w \approx 600$), tetraethyl orthosilicate (TEOS), copper sulfate pentahydrate ($CuSO_4{\cdot}5H_2O$), dextran ($M_w \sim 150{,}000$ from *Leuconostoc mesenteroides*), and sodium hydroxide were purchased from Sigma-Aldrich. Hydrochloric acid (HCl, 37%) and sodium hydroxide (NaOH) were purchased from Fisher Scientific. Ultrapure water (Arium Pro UV water purification system) with a resistivity of 18.2 MΩ cm was used for all experiments.

2.2. PDA Coatings. Silicon wafers (WaferNet, San Jose, USA) were first rinsed with acetone, ethanol, and ultrapure water and then dried by a stream of compressed dry air. The wafers were next plasma-cleaned (PDC-32G plasma cleaner, Harrick Plasma) using high power under a constant water vapor pressure of 500 mTorr for 30 s. The thickness of the silica layer was then measured by spectroscopic ellipsometry. DA was dissolved in Tris buffer solution (pH = 8.5, 50 mM), and the silicon wafers were immersed in the DA solution (2 mg mL^{-1}) and stirred at 250 rpm. To keep the individual sample surfaces fixed and vertically aligned, the wafers were mounted into a costume-made Teflon holder (Section S1). Coatings were deposited using the common one-step method or the LbL approach. In the former, the silicon wafers were immersed in the DA solution for a certain duration. Afterward, the silicon wafer was removed from the solution, rinsed with Tris buffer, sonicated in fresh Tris buffer for 1 min, and dried by compressed airflow. The ultrasonic cleaning procedure was repeated three times to ensure the removal of weakly attached PDA aggregates. In the LbL approach, the DA solution was exchanged with a fresh solution every 2 h. For example, a total deposition time of 12 h comprised 6 × 2 h deposition steps. Between each deposition step, the samples were sonicated and dried as described above. Three replicas were prepared for each sample. Additionally, coatings were also obtained by 2 × 6 h depositions and a 12 h one-step deposition (Section S2).

2.3. PDA-Dextran and PDA-PEI Coatings. Dextran (10 mg mL^{-1}) was first fully dissolved in Tris buffer (pH = 8.5, 50 mM), and then DA (2 mg mL^{-1}) was added and dissolved in the dextran solution. One-step and LbL deposition methods were then used to prepare PDA-dextran hybrid coatings. PDA-PEI hybrid coatings were deposited similarly using PEI and DA concentrations of 0.2 and 2 mg mL^{-1}, respectively.

2.4. PDA-Based Hierarchical Coating. The LbL procedure consisted of five steps, where in each step, a layer with specific composition was deposited. The silica wafer was first immersed in DA (2 mg mL^{-1}) solution and then was immersed in mixed solutions of DA-PEI (2 and 0.2 mg mL^{-1}),[18] DA-TEOS (2 and 42 mg mL^{-1}),[11] DA-$CuSO_4{\cdot}5H_2O$ (2 and 0.3 mg mL^{-1}),[37] and DA-dextran (2 and 10 mg mL^{-1}),[38] respectively. All the solutions were prepared in Tris buffer (pH = 8.5, 50 mM). Each deposition step was 2 h, and between the steps, the samples were sonicated and dried as described above.

2.5. Atomic Force Microscopy. Atomic force microscopy (AFM, NanoWizard 3, JPK Instruments AG, Berlin, Germany) operating in tapping mode in air was used to obtain topographical images and to estimate the thickness of the coatings (scratching test). The topographical images were collected with a scan rate of 0.2 Hz, a pixel resolution of 128 × 128, a scan area of 10 × 10 μm^2, and a standard tapping mode cantilever (HQ: NSC5/AL BS, tip radius of 8 nm, k = 40 N/m, Mikromasch, USA). For each sample, a total number of nine AFM height images (three randomly-selected areas on three replicas) were obtained. Root mean square roughness (R_q) was next calculated from the AFM images (a polynomial fit was subtracted from each scan line independently) using the standard software of the instrument (JPK SPM Data Processing). To reduce the influence of error from the randomly chosen surface positions, the smallest and largest values of the roughness were eliminated, and the reported R_q values are thus the average of seven values for each sample. For the thickness evaluation, the coatings were carefully scratched using a tweezer, and AFM images were collected over the scratched area (scan rate of 0.1 Hz).

2.6. Spectroscopic Ellipsometry. Spectroscopic ellipsometry (M-2000X, J.A. Woollam Co., Inc.) measurements were performed to assess the thickness and optical properties of the coatings. The ellipsometric ψ (amplitude ratio) and Δ (phase shift) were collected in air in the wavelength range of 245−1000 nm at 5 different angles of incidence (50, 55, 60, 65, and 70°). For each sample, a total number of 15 measurements (five randomly-selected spots on three replicas) were conducted. Depending on the deposition time, different optical models were used to describe the optical behavior of the coatings,[39] namely, Cauchy with Urbach absorption for short depositions, B-spline for intermediate depositions, and B-spline with a roughness layer for long depositions (Section S3).

https://doi.org/10.1021/acsomega.2c05620
ACS Omega 2023, 8, 2965−2972

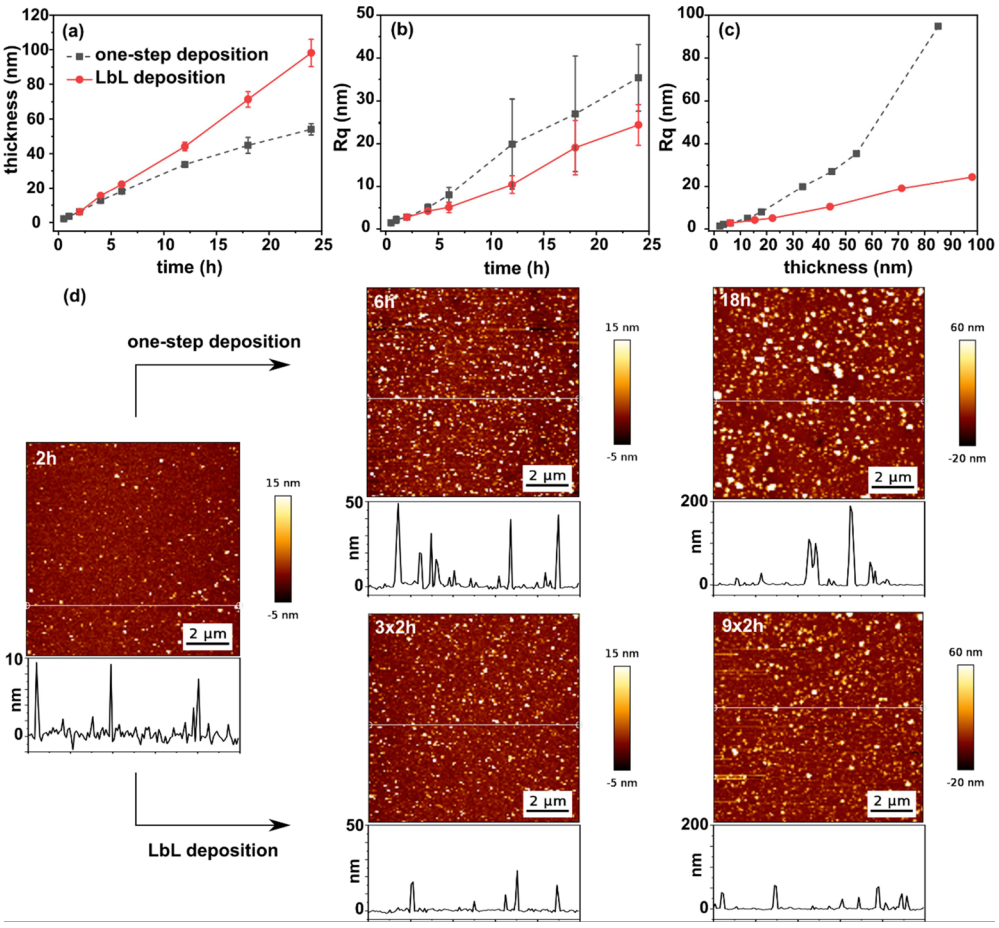

Figure 1. PDA coatings obtained by one-step and LbL deposition methods: (a) ellipsometry thickness vs deposition time (n = 15). (b) Root-mean-square roughness (R_q) vs deposition time (n = 7) calculated over 10 × 10 μm^2 area. (c) R_q vs ellipsometry thickness. (d) Representative AFM images and corresponding height profiles of PDA films.

2.7. X-ray Photoelectron Spectroscopy. To analyze the chemical composition of the PDA-based coatings, angle-resolved X-ray photoelectron spectroscopy (XPS, Nexsa, Thermo Fisher Scientific, USA) measurements were performed with a monochromated Al K-alpha source (1486.6 eV) and a flood gun for charge compensation. For each sample, three random points were characterized and analyzed using Avantages software.

2.8. Zeta Potential. Zeta potential (SurPASS3, Anton Paar GmbH, Austria) measurements were conducted to evaluate the charge properties of coatings. Two samples (2 × 1 cm) were mounted into the instrument flow cell separated by a 100 ± 5 μm capillary channel. The solution (1 mM NaCl) was pumped through the capillary channel between the two samples, producing a linearly decreasing measurement pressure (600–400 mbar). The measurements were conducted in two pH conditions (3 and 9). To ensure the reliability of the data, the measurements were repeated five times in each condition.

2.9. Stability of PDA Films. The stability of the PDA coatings, prepared by one-step and LBL deposition, was assessed according to a previously reported approach.[40] Briefly, PDA coatings (made by one-step 6 h deposition and 3 × 2 h LbL depositions) were immersed in (i) HCl solution (pH = 1) for 24 h and (ii) NaOH solution (pH = 13) for 0.5 h. The ellipsometric thickness of the coatings before and after acid/base treatment was measured to examine the stability of the coatings.

3. RESULTS AND DISCUSSION

3.1. LbL Deposition of PDA. PDA coatings were constructed using the LbL approach to investigate how it can provide control of the growth rate and the morphology of the coatings. To do so, the substrate was immersed in a fresh DA solution for 2 h, rinsed to remove the loosely bound aggregates, and then immersed in a fresh DA solution. This cyclic process was repeated several times to obtain coatings of varying thicknesses. In Figure 1a,b, the thickness of the coatings, obtained by ellipsometry, and the surface roughness (R_q) of the coatings, obtained by AFM, are directly compared to the values for PDA coatings obtained by the common one-step deposition method (i.e., DA solution is not exchanged with a fresh solution). For the one-step method, the coating thickness linearly grows for deposition times up to 12 h, after which it starts to flatten out. Such a decaying growth is in agreement with the literature observations, which has been attributed to the consumption of DA and the formation of excessively large aggregates (>∼50 nm) in the aged solution.[41] The thickness of the PDA coatings obtained by the LbL method (for the same total deposition time) is, however, relatively larger, for example, the average thickness from a one-step deposition for 24 h is ∼50 nm, whereas 12 × 2 h LbL depositions yield a thickness of ∼100 nm. In addition, a linear growth behavior is obtained when using the LbL approach, suggesting a roughly constant adsorbed amount through each deposition step.

https://doi.org/10.1021/acsomega.2c05620
ACS Omega 2023, 8, 2965−2972

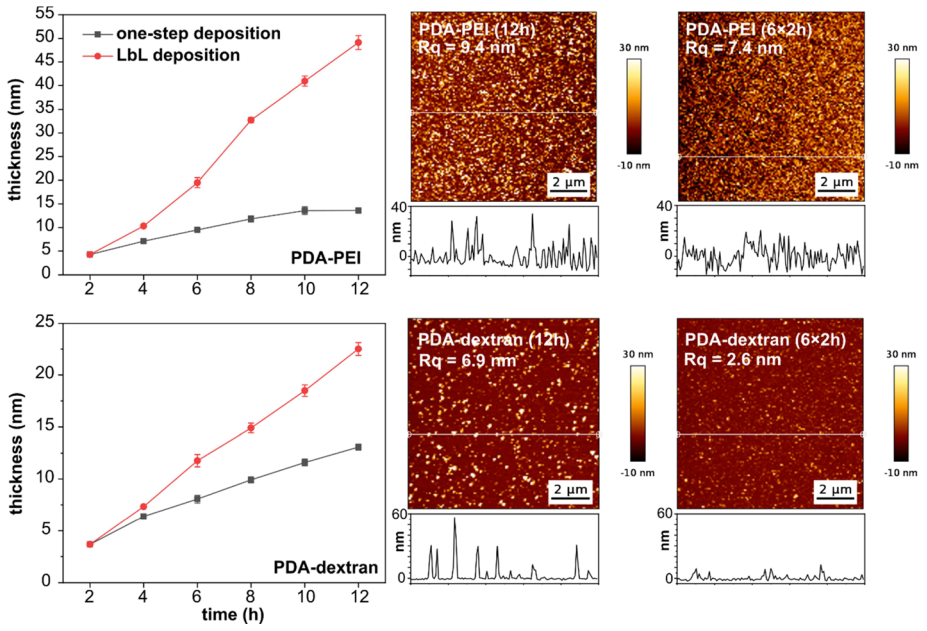

Figure 2. PDA-polymer hybrid coatings obtained by one-step and LbL deposition methods: (top row) PDA-PEI coatings (bottom row) and PDA-dextran coatings.

Table 1. Elemental Composition of Hybrid PDA-Polymer Coatings Obtained by One-Step and LbL Deposition Methods

	C (%)	N (%)	O (%)	Si (%)	C/N
PDA-dextran (12 h)	65.7 ± 0.3	7.4 ± 0.3	25.5 ± 0.1	1.4 ± 0.1	8.9 ± 0.4
PDA-dextran (6 × 2 h)	68.9 ± 0.3	6.6 ± 0.2	24.5 ± 0.2		10.5 ± 0.4
PDA-PEI (12 h)	69.2 ± 0.3	14.8 ± 0.3	14.5 ± 0.2	1.5 ± 0	4.7 ± 0.1
PDA-PEI (6 × 2 h)	72.6 ± 0.4	14.4 ± 0.4	13.0 ± 0.1		5.1 ± 0.2

Regarding surface morphology (Figure 1b), in both methods, R_q is found to generally increase with the deposition time; however, surface aggregation is reduced by the LbL approach, as shown in AFM images and corresponding height profiles (also see Section S4). For instance, the coating obtained by 18 h one-step deposition contains surface aggregates of ∼5 to 200 nm height. The relatively large standard deviation of the calculated R_q herein can also suggest the heterogeneous nature of the surface. For 9 × 2 h LbL depositions, the size of the aggregated domains is found to be much smaller, that is, ∼5 to 50 nm. The benefit of using the LbL approach on coating thickness/morphology can be better perceived from Figure 1c, where the R_q-values are plotted against the coating thicknesses. Accordingly, the surface roughness increases exponentially with the coating thickness for the one-step method, whereas the LbL approach provides a moderate linear correlation.

In addition, the stability of the PDA films obtained by one-step and LbL deposition were assessed in HCl (pH = 1) and NaOH (pH = 13) solutions (Section S5), suggesting that the coatings made by the LbL approach are relatively more resistant.

3.2. LbL Co-Deposition of PDA and Polymers. DA-quinone oligomers can form various covalent (e.g., Schiff base and Michael addition) and non-covalent (e.g., hydrogen bonding and coordination) interactions with polymers, nanoparticles, and metal ions.[8] Benefiting from this versatile chemistry, co-deposition of DA and other materials, that is, DA-assisted deposition, thus allows entrapping functional units within a PDA coating to yield desired bulk and surface properties. We herein investigated to what extent the LbL approach can provide control over the growth behavior and the surface morphology of PDA-polymer hybrid coatings. To do so, two model polymers, that is, PEI and dextran, were selected, which represent covalent and non-covalent DA-assisted depositions.

PEI is a cationic polymer rich in amine groups that can form covalent (Schiff base and Michael addition) interactions with the quinone derivatives.[18,42] In a mixed solution of DA and PEI, PDA-PEI aggregates grow with time and simultaneously adhere to the substrate, providing PDA-PEI hybrid coatings. PEI, by reacting with the quinone derivatives, interrupts PDA-PDA hydrogen bonding and $\pi-\pi$ stacking interactions; thus, hindering excessive PDA aggregation. Therefore, PDA-PEI hybrid coatings in general are thinner with smoother surface morphologies, compared with PDA coatings.[18] Herein, PDA-PEI hybrid coatings were prepared using one-step and LbL deposition methods (Figure 2, top row). Using the one-step deposition method, a decaying growth rate is found, and the thickness reaches a plateau of ∼12 nm after 10 h. The surface morphology of the coating is found to be relatively smooth (R_q = 9.1 ± 0.7 nm) compared with PDA coatings (R_q = 19.9 ± 0.7 nm), yet surface aggregates of ∼5 to 40 nm height are still present (for 12 h deposition). The LbL approach provides a linear growth behavior where the coating thickness reaches ∼50 nm after 6 × 2 h depositions. The surface morphology herein is also found to be smoother (7.7 ± 0.4 nm), as the size of aggregates is reduced to ∼5 to 20 nm. The elemental composition (Table 1) of PDA-PEI coatings prepared by one-step and LbL depositions show a rather similar C/N ratio for both coatings, thus suggesting a rather similar chemical composition in both cases.

https://doi.org/10.1021/acsomega.2c05620
ACS Omega 2023, 8, 2965−2972

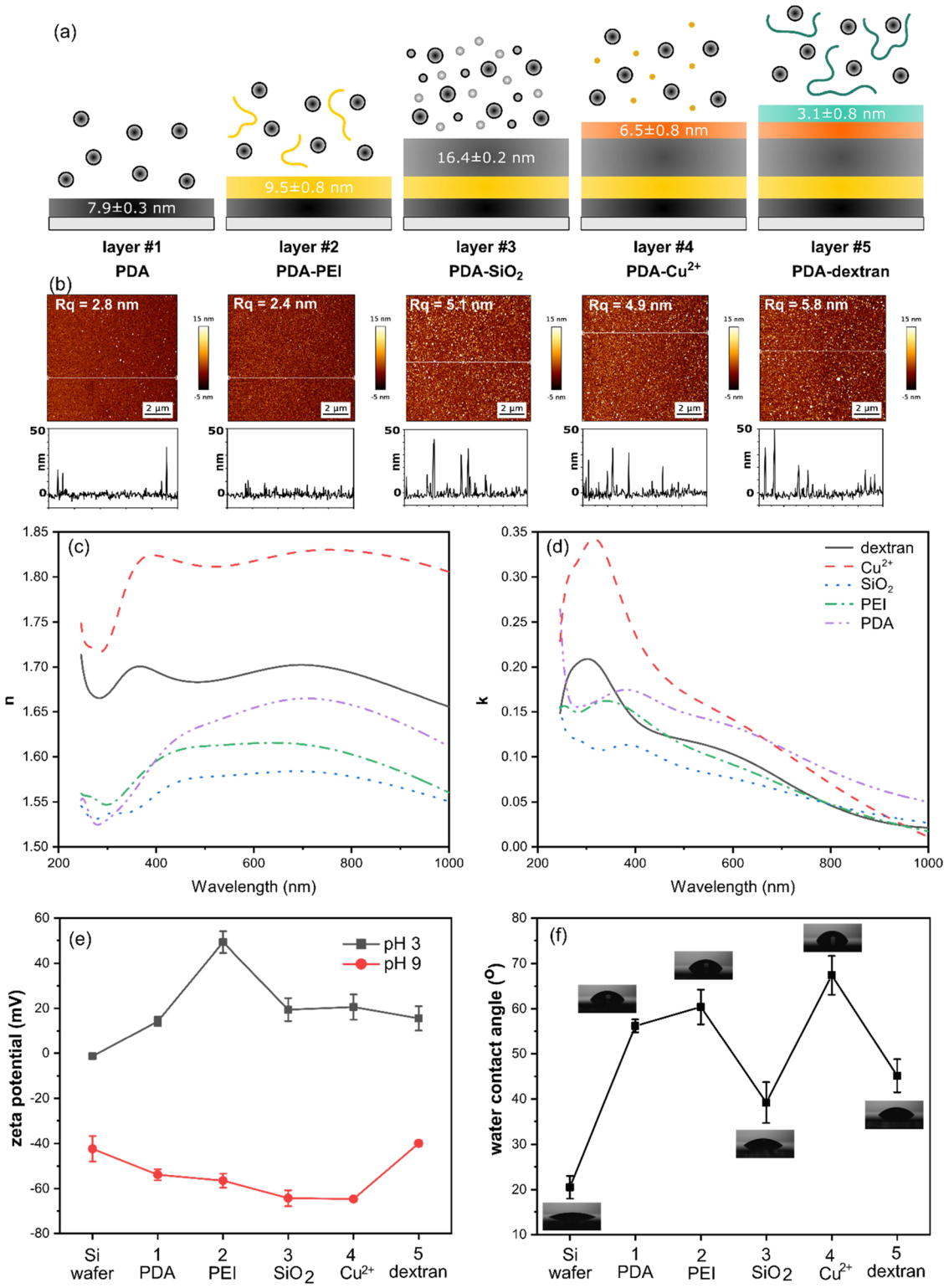

Figure 3. Hierarchical multilayer coating obtained by LbL depositions (2 h) of DA, DA-PEI, DA-TEOS, DA-$CuSO_4$, and DA-dextran on a silica substrate; (a) schematic illustration of the multilayer structure and thickness of each layer calculated by ellipsometry ($n = 3$), (b) representative AFM images and corresponding height profiles of the multilayer coating after each deposition, (c, d) modeled refractive index (n) and extinction coefficient of each layer from ellipsometry, (e) surface zeta potential after each deposition, and (f) water contact angle after each deposition.

Dextran is a polysaccharide with a backbone rich in hydroxyl and ether groups that can form hydrogen bonds with DA oligomers.[38] Therefore, dextran can be incorporated into the coating by non-covalent hydrogen bonding interactions. Similar to the case of PDA-PEI, it has been suggested that dextran also can prevent excessive aggregation of PDA by inhibiting the noncovalent assembly routes. PDA-dextran coatings were herein prepared by one-step and LbL deposition methods. For the one-step deposition method, rather linear growth is found where the coating thickness after 12 h reaches ~12 nm. The coating shows

https://doi.org/10.1021/acsomega.2c05620
ACS Omega 2023, 8, 2965−2972

Table 2. Elemental Composition for Hierarchical Multilayer Coating after Deposition of Each Layer

	C (%)	N (%)	O (%)	Si (%)	Cu (%)	C/N	C/O
PDA	58.0 ± 1.8	7.5 ± 0.1	26.4 ± 0.9	8.1 ± 0.8		7.7 ± 0.3	2.2 ± 0.1
PDA-PEI	67.3 ± 0.4	13.2 ± 0.2	18.1 ± 0.2	1.4 ± 0.1		5.1 ± 0.1	3.7 ± 0.1
PDA-SiO_2	38.3 ± 0.7	4.6 ± 0.2	41.7 ± 0.3	15.4 ± 0.5		8.3 ± 0.3	0.9 ± 0.1
PDA-Cu^{2+}	67.3 ± 0.1	8.2 ± 0.2	22.5 ± 0.1	1.4 ± 0.1	0.6 ± 0.1	8.2 ± 0.2	3.0 ± 0.1
PDA-dextran	68.7 ± 0.3	7.1 ± 0.3	24.2 ± 0.3			9.6 ± 0.4	2.8 ± 0.1

a relatively rough surface morphology (R_q = 5.1 ± 0.9 nm), where aggregates of ∼5 to 60 nm are observed. LbL deposition is found to both increase the film thickness and significantly reduce the surface roughness (R_q = 3.6 ± 1 nm), that is, surface heights <10 nm. The elemental composition of the two coatings is also found to be relatively similar according to the XPS analysis (Table 1).

In summary, our data demonstrate that the LbL approach allows preparing hybrid PDA-polymer coatings with enhanced thickness and reduced surface roughness. This approach is found to be effective for both cases of covalent and non-covalent co-depositions.

3.3. Hierarchically Layered Coating. The benefits of combining the DA-assisted deposition with the LbL approach are not limited to increased coating thickness and reduced surface aggregation. This combination enables vast possibilities to construct hierarchal composite coatings where the compositions and functional properties can be tuned in the Z-direction (perpendicular to the substrate). As a proof of concept, we herein constructed a model coating comprising five different layers by LbL deposition of (i) PDA, (ii) PDA-PEI, (iii) PDA-SiO_2, (iv) PDA-Cu^{2+}, and (v) PDA-dextran. These different materials (polyelectrolyte, inorganic compound, metal ion, and uncharged polymer) associate with DA-quinone oligomers via different interactions (covalent bonds, hydrogen bonding, and coordination bonds). By constructing such a layer, we thus aimed to demonstrate the versatility of the proposed LbL approach.

Figure 3 summarizes the examined properties of the multilayer coating following each deposition step. Table 2 summarizes the elemental composition of the coating after each deposition step, which confirms the incorporation of the co-deposited units in each step. Clear variations in the properties of the coating are found after each deposition step, which affirms how each deposition step allows tuning the coating properties. Variations in the surface topography (Figure 3b) are found after each deposition step. For instance, when the PDA-PEI layer is deposited (layer #2), rather smooth surface morphology is achieved. On the other hand, the PDA-SiO_2 layer produces a rather heterogeneous surface morphology due to PDA aggregates or entrapped nanoparticles. Overall though, the final multilayer coating has a relatively smooth surface owing to the LbL approach. The combination of LbL and DA-assisted deposition herein thus provides the possibility to modulate the surface roughness of composite coatings, for example, through (i) deposition of an intrinsically smooth hybrid layer such as PDA-PEI, as shown in Figure 3b, or (ii) a shorter deposition of a desired hybrid layer as the top layer. From the ellipsometry measurements (Section S6), the optical constants of each deposited layer were also estimated (Figure 3c,d). It should be noted that the values of n and k herein are not directly measured but obtained from a modeling analysis; hence, some degree of uncertainty in the absolute values and shape of the optical dispersions is inevitable. Yet, comparing the different layers with each other, variations in the optical constants are noticeable, which originates from different chemical compositions of the layers. For instance, the layer containing Cu^{2+} shows relatively larger values of n and k, while the next deposited layer including dextran has reduced values of n and k.

Surface charge is another parameter that showed large dependence on the deposited layers. We measured this parameter in both acidic and alkaline pH to better see the effects of protonation/deprotonation of the incorporated ionizable groups (Figure 3e). Starting from the bare silica substrate, one can expect only minor deprotonation of the silanol groups at acidic pH and notable deprotonation toward higher pH, which is confirmed by a negative near-zero zeta potential at pH 3 and a large negative surface potential at pH 9. Having PDA deposited as the first layer, a more cationic surface at pH 3 and a more anionic surface at pH 9 are found due to the ionization of amine and carboxyl groups found in PDA particles. When the next layer containing PEI is deposited, the surface charge at pH 3 becomes significantly more positively charged due to the amine-rich and cationic nature of PEI. Deposition of the third layer produced an overall shift to a more negatively charged surface, resulting from the negatively charged groups on both DA and SiO_2. While the fourth layer with copper ions does not alter the surface charge notably, the last layer including dextran showed reduced surface charge (in magnitude) possibly due to the incorporation of uncharged dextran molecules. Aside from the general trends demonstrated here, the surface charge is a key parameter that greatly matters when dealing with adsorption, binding, or adhesion of charged molecules and particles to a surface, for instance, in designing anti-fouling coatings or cell-adhesive substrates. Herein, the ability to readily tune the surface charge of the coating using the LbL approach can provide great control of the surface interactions/properties.[43] In the same line, hydrophilicity (wettability) is another important surface property of a coating.[44] Herein, the surface hydrophilicity (Figure 3f) of the multilayer coating was also shown to greatly depend on each deposited layer. Silica being highly hydrophilic showed an expected contact angle of ∼20°. PDA added as the first layer made the surface more hydrophobic, increasing the contact angle to ∼55°. In the same line, depending on the chemistry of the deposited units, the surface hydrophilicity of the coating was shown to be easily adjustable using the LbL approach. For instance, layers including hydrophilic units such as SiO_2 or dextran were shown to reduce the contact angle notably.

4. SUMMARY AND CONCLUSIONS

A combination of DA-assisted deposition with the LbL approach allows for constructing functional coatings with tunable thickness, roughness, and chemical composition. The versatile catechol chemistry herein enables the incorporation of various materials into the coating. On the other hand, the LbL approach allows extending the thickness of the coating, reducing the surface aggregation, and finally varying the composition and

https://doi.org/10.1021/acsomega.2c05620
ACS Omega 2023, 8, 2965−2972

properties of the coating in the vertical direction as desired. Such "lego-like" construction provides infinite possibilities for constructing composite coatings, where the chemistry and functional properties can be tuned at the coating−substrate interface, within the coating bulk, and at the coating surface.

■ ASSOCIATED CONTENT

Supporting Information

The Supporting Information is available free of charge at https://pubs.acs.org/doi/10.1021/acsomega.2c05620.

Experimental setup for coating preparation, AFM and ellipsometry data for 12 h one-step deposition and 2 × 6 h LbL depositions, detailed ellipsometry data modeling, additional AFM images, and stability analysis of coatings in acid/base (PDF)

■ AUTHOR INFORMATION

Corresponding Author

Esben Thormann − *Department of Chemistry, Technical University of Denmark, 2800 Kgs. Lyngby, Denmark;* orcid.org/0000-0002-2364-3493; Email: esth@kemi.dtu.dk

Authors

Runtian Qie − *Department of Chemistry, Technical University of Denmark, 2800 Kgs. Lyngby, Denmark;* orcid.org/0000-0002-6206-884X

Saeed Zajforoushan Moghaddam − *Department of Chemistry, Technical University of Denmark, 2800 Kgs. Lyngby, Denmark;* orcid.org/0000-0002-6536-7490

Complete contact information is available at: https://pubs.acs.org/10.1021/acsomega.2c05620

Notes

The authors declare no competing financial interest.

■ ACKNOWLEDGMENTS

R.Q. acknowledges the scholarship from the China Scholarship Council.

■ REFERENCES

(1) Lee, H.; Dellatore, S. M.; Miller, W. M.; Messersmith, P. B. Mussel-Inspired Surface Chemistry for Multifunctional Coatings. *Science* **2007**, *318*, 426−430.

(2) Yang, H.-C.; Luo, J.; Lv, Y.; Shen, P.; Xu, Z.-K. Surface Engineering of Polymer Membranes via Mussel-Inspired Chemistry. *J. Memb. Sci.* **2015**, *483*, 42−59.

(3) Liu, R.; Fu, X.; Wang, C.; Dawson, G. Dopamine Surface Modification of Trititanate Nanotubes: Proposed In-Situ Structure Models. *Chem. −A Eur. J.* **2016**, *22*, 6071−6074.

(4) Dreyer, D. R.; Miller, D. J.; Freeman, B. D.; Paul, D. R.; Bielawski, C. W. Elucidating the Structure of Poly(Dopamine). *Langmuir* **2012**, *28*, 6428−6435.

(5) Hong, S.; Wang, Y.; Park, S. Y.; Lee, H. Progressive Fuzzy Cation-π Assembly of Biological Catecholamines. *Sci. Adv.* **2018**, *4*, No. eaat7457.

(6) Kang, S. M.; Hwang, N. S.; Yeom, J.; Park, S. Y.; Messersmith, P. B.; Choi, I. S.; Langer, R.; Anderson, D. G.; Lee, H. One-Step Multipurpose Surface Functionalization by Adhesive Catecholamine. *Adv. Funct. Mater.* **2012**, *22*, 2949−2955.

(7) Yang, H.-C.; Pi, J.-K.; Liao, K.-J.; Huang, H.; Wu, Q.-Y.; Huang, X.-J.; Xu, Z.-K. Silica-Decorated Polypropylene Microfiltration Membranes with a Mussel-Inspired Intermediate Layer for Oil-in-Water Emulsion Separation. *ACS Appl. Mater. Interfaces* **2014**, *6*, 12566−12572.

(8) Qiu, W.-Z.; Yang, H.-C.; Xu, Z.-K. Dopamine-Assisted Co-Deposition: An Emerging and Promising Strategy for Surface Modification. *Adv. Colloid Interface Sci.* **2018**, *256*, 111−125.

(9) Zhang, Y.; Thingholm, B.; Goldie, K. N.; Ogaki, R.; Städler, B. Assembly of Poly(Dopamine) Films Mixed with a Nonionic Polymer. *Langmuir* **2012**, *28*, 17585−17592.

(10) Ma, M.-Q.; Zhang, C.; Chen, T.-T.; Yang, J.; Wang, J.-J.; Ji, J.; Xu, Z.-K. Bioinspired Polydopamine/Polyzwitterion Coatings for Underwater Anti-Oil and -Freezing Surfaces. *Langmuir* **2019**, *35*, 1895−1901.

(11) Ho, C.-C.; Ding, S.-J. Novel SiO 2 /PDA Hybrid Coatings to Promote Osteoblast-like Cell Expression on Titanium Implants. *J. Mater. Chem. B* **2015**, *3*, 2698−2707.

(12) Son, H. Y.; Ryu, J. H.; Lee, H.; Nam, Y. S. Silver-Polydopamine Hybrid Coatings of Electrospun Poly(Vinyl Alcohol) Nanofibers. *Macromol. Mater. Eng.* **2013**, *298*, 547−554.

(13) Zhu, J.; Tsehaye, M. T.; Wang, J.; Uliana, A.; Tian, M.; Yuan, S.; Li, J.; Zhang, Y.; Volodin, A.; Van der Bruggen, B. A Rapid Deposition of Polydopamine Coatings Induced by Iron (III) Chloride/Hydrogen Peroxide for Loose Nanofiltration. *J. Colloid Interface Sci.* **2018**, *523*, 86−97.

(14) Wang, Z.; Zou, Y.; Li, Y.; Cheng, Y. Metal-Containing Polydopamine Nanomaterials: Catalysis, Energy, and Theranostics. *Small* **2020**, *16*, No. 1907042.

(15) Bernsmann, F.; Ball, V.; Addiego, F.; Ponche, A.; Michel, M.; de Gracio, J. J. A.; Toniazzo, V.; Ruch, D. Dopamine−Melanin Film Deposition Depends on the Used Oxidant and Buffer Solution. *Langmuir* **2011**, *27*, 2819−2825.

(16) Ponzio, F.; Barthès, J.; Bour, J.; Michel, M.; Bertani, P.; Hemmerlé, J.; D'Ischia, M.; Ball, V. Oxidant Control of Polydopamine Surface Chemistry in Acids: A Mechanism-Based Entry to Superhydrophilic-Superoleophobic Coatings. *Chem. Mater.* **2016**, *28*, 4697−4705.

(17) Trzcińska, Z.; Bruggeman, M.; Ijakipour, H.; Hodges, N. J.; Bowen, J.; Stamboulis, A. Polydopamine Linking Substrate for AMPs: Characterisation and Stability on Ti6Al4V. *Materials* **2020**, *13*, 3714.

(18) Lv, Y.; Yang, S.-J.; Du, Y.; Yang, H.-C.; Xu, Z.-K. Co-Deposition Kinetics of Polydopamine/Polyethyleneimine Coatings: Effects of Solution Composition and Substrate Surface. *Langmuir* **2018**, *34*, 13123−13131.

(19) Ball, V.; Del Frari, D.; Toniazzo, V.; Ruch, D. Kinetics of Polydopamine Film Deposition as a Function of PH and Dopamine Concentration: Insights in the Polydopamine Deposition Mechanism. *J. Colloid Interface Sci.* **2012**, *386*, 366−372.

(20) Richardson, J. J.; Björnmalm, M.; Caruso, F. Technology-Driven Layer-by-Layer Assembly of Nanofilms. *Science* **2015**, *348*, aaa2491−aaa2491.

(21) Guzmán, E.; Rubio, R. G.; Ortega, F. A Closer Physico-Chemical Look to the Layer-by-Layer Electrostatic Self-Assembly of Polyelectrolyte Multilayers. *Adv. Colloid Interface Sci.* **2020**, *282*, No. 102197.

(22) Richardson, J. J.; Cui, J.; Björnmalm, M.; Braunger, J. A.; Ejima, H.; Caruso, F. Innovation in Layer-by-Layer Assembly. *Chem. Rev.* **2016**, *116*, 14828−14867.

(23) Srivastava, S.; Kotov, N. A. Composite Layer-by-Layer (LBL) Assembly with Inorganic Nanoparticles and Nanowires. *Acc. Chem. Res.* **2008**, *41*, 1831−1841.

(24) Heath, G. R.; Li, M.; Polignano, I. L.; Richens, J. L.; Catucci, G.; O'Shea, P.; Sadeghi, S. J.; Gilardi, G.; Butt, J. N.; Jeuken, L. J. C. Layer-by-Layer Assembly of Supported Lipid Bilayer Poly-L-Lysine Multilayers. *Biomacromolecules* **2016**, *17*, 324−335.

(25) Kim, B.-S.; Park, S. W.; Hammond, P. T. Hydrogen-Bonding Layer-by-Layer-Assembled Biodegradable Polymeric Micelles as Drug Delivery Vehicles from Surfaces. *ACS Nano* **2008**, *2*, 386−392.

(26) An, Q.; Huang, T.; Shi, F. Covalent Layer-by-Layer Films: Chemistry, Design, and Multidisciplinary Applications. *Chem. Soc. Rev.* **2018**, *47*, 5061−5098.

(27) Bernsmann, F.; Ersen, O.; Voegel, J.-C.; Jan, E.; Kotov, N. A.; Ball, V. Melanin-Containing Films: Growth from Dopamine Solutions versus Layer-by-Layer Deposition. *ChemPhysChem* **2010**, *11*, 3299−3305.

(28) Ma, X.; Wu, G.; Dai, F.; Li, D.; Li, H.; Zhang, L.; Deng, H. Chitosan/Polydopamine Layer by Layer Self-Assembled Silk Fibroin Nanofibers for Biomedical Applications. *Carbohydr. Polym.* **2021**, *251*, No. 117058.
(29) Ou, J.; Wang, J.; Qiu, Y.; Liu, L.; Yang, S. Mechanical Property and Corrosion Resistance of Zirconia/Polydopamine Nanocomposite Multilayer Films Fabricated via a Novel Non-Electrostatic Layer-by-Layer Assembly Technique. *Surf. Interface Anal.* **2011**, *43*, 803−808.
(30) Xie, C.; Lu, X.; Wang, K.; Yuan, H.; Fang, L.; Zheng, X.; Chan, C.; Ren, F.; Zhao, C. Pulse Electrochemical Driven Rapid Layer-by-Layer Assembly of Polydopamine and Hydroxyapatite Nanofilms via Alternative Redox in Situ Synthesis for Bone Regeneration. *ACS Biomater. Sci. Eng.* **2016**, *2*, 920−928.
(31) Papananou, H.; Katsumata, R.; Neary, Z.; Goh, R.; Meng, X.; Limary, R.; Segalman, R. A. Dopamine-Mediated Polymer Coating Facilitates Area-Selective Atomic Layer Deposition. *ACS Appl. Polym. Mater.* **2021**, *3*, 4924−4931.
(32) Wang, D.; Ha, Y.; Gu, J.; Li, Q.; Zhang, L.; Yang, P. 2D Protein Supramolecular Nanofilm with Exceptionally Large Area and Emergent Functions. *Adv. Mater.* **2016**, *28*, 7414−7423.
(33) Wu, Z.; Yang, P. Simple Multipurpose Surface Functionalization by Phase Transited Protein Adhesion. *Adv. Mater. Interfaces* **2015**, *2*, No. 1400401.
(34) Xu, Y.; Liu, Y.; Hu, X.; Qin, R.; Su, H.; Li, J.; Yang, P. The Synthesis of a 2D Ultra-Large Protein Supramolecular Nanofilm by Chemoselective Thiol−Disulfide Exchange and Its Emergent Functions. *Angew. Chem. Int. Ed.* **2020**, *59*, 2850−2859.
(35) Follmann, H. D. M.; Naves, A. F.; Martins, A. F.; Félix, O.; Decher, G.; Muniz, E. C.; Silva, R. Advanced Fibroblast Proliferation Inhibition for Biocompatible Coating by Electrostatic Layer-by-Layer Assemblies of Heparin and Chitosan Derivatives. *J. Colloid Interface Sci.* **2016**, *474*, 9−17.
(36) Jiang, T.; Moghaddam, S. Z.; Thormann, E. A PH-Responsive Polyelectrolyte Multilayer Film with Tunable Interfacial Properties. *Polymer* **2021**, *214*, No. 123367.
(37) Gao, R.; Zhang, L.; Hao, Y.; Cui, X.; Liu, D.; Zhang, M.; Tang, Y. One-Step Preparation of Magnetic Imprinted Nanoparticles Adopting Dopamine-Cupric Ion as a Co-Monomer for the Specific Recognition of Bovine Hemoglobin. *J. Sep. Sci.* **2015**, *38*, 3568−3574.
(38) Liu, Y.; Chang, C.-P.; Sun, T. Dopamine-Assisted Deposition of Dextran for Nonfouling Applications. *Langmuir* **2014**, *30*, 3118−3126.
(39) Qie, R.; Zajforoushan Moghaddam, S.; Thormann, E. Parameterization of the Optical Constants of Polydopamine Films for Spectroscopic Ellipsometry Studies. *Phys. Chem. Chem. Phys.* **2021**, *23*, 5516−5526.
(40) Bernsmann, F.; Ponche, A.; Ringwald, C.; Hemmerlé, J.; Raya, J.; Bechinger, B.; Voegel, J.-C.; Schaaf, P.; Ball, V. Characterization of Dopamine−Melanin Growth on Silicon Oxide. *J. Phys. Chem. C* **2009**, *113*, 8234−8242.
(41) Zhu, B.; Edmondson, S. Polydopamine-Melanin Initiators for Surface-Initiated ATRP. *Polymer* **2011**, *52*, 2141−2149.
(42) Luo, R.; Wang, X.; Deng, J.; Zhang, H.; Maitz, M. F.; Yang, L.; Wang, J.; Huang, N.; Wang, Y. Dopamine-Assisted Deposition of Poly (Ethylene Imine) for Efficient Heparinization. *Colloids Surf. B Biointerfaces* **2016**, *144*, 90−98.
(43) Brett, C. J.; Mittal, N.; Ohm, W.; Gensch, M.; Kreuzer, L. P.; Körstgens, V.; Månsson, M.; Frielinghaus, H.; Müller-Buschbaum, P.; Söderberg, L. D.; Roth, S. V. Water-Induced Structural Rearrangements on the Nanoscale in Ultrathin Nanocellulose Films. *Macromolecules* **2019**, *52*, 4721−4728.
(44) Chen, Q.; Brett, C. J.; Chumakov, A.; Gensch, M.; Schwartzkopf, M.; Körstgens, V.; Söderberg, L. D.; Plech, A.; Zhang, P.; Müller-Buschbaum, P.; Roth, S. V. Layer-by-Layer Spray-Coating of Cellulose Nanofibrils and Silver Nanoparticles for Hydrophilic Interfaces. *ACS Appl. Nano Mater.* **2021**, *4*, 503−513.

https://doi.org/10.1021/acsomega.2c05620
ACS Omega 2023, 8, 2965−2972